Construction and Building Materials 142 (2017) 536–551

Contents lists available at ScienceDirect

Construction and Building Materials

journal homepage: www.elsevier.com/locate/conbuildmat

Artificial ageing of glass with sand abrasion

Kyriaki Corinna Datsiou *, Mauro Overend

Glass and Façade Technology Research Group, Department of Engineering, University of Cambridge, Cambridge CB2 1PZ, UK

HIGHLIGHTS

- Naturally aged glass was found to be significantly weaker than as-received glass.
- Falling abrasive was investigated as an artificial ageing method for glass.
- The naturally aged glass was used as a reference for the falling abrasive method.
- Existing falling abrasive standards proved unsafe due to overestimation of design strength.
- Alternative ageing parameters offer good correlation to naturally aged glass strength.

ARTICLE INFO

Article history:
Received 23 September 2016
Received in revised form 3 February 2017
Accepted 11 March 2017
Available online 21 March 2017

Keywords:
Artificially aged glass
Naturally aged glass
Falling abrasive/sand trickling method
Erosive resistance of glass
Glass strength
Long term mechanical performance of glass

ABSTRACT

The strength of glass is governed by the condition of its surface which deteriorates progressively as surface flaws accumulate on exposure to weathering action during its service life. Therefore, knowledge of the strength of naturally aged glass is crucial in order to ensure its safe use in load-bearing applications. Artificial ageing tests can be very useful in this regard, but they have traditionally focused on degradation in light transmittance properties rather than the strength of glass. Experimental testing has been undertaken in this study to investigate the effectiveness of a falling abrasive method for the artificial ageing of glass. Abrasive medium is allowed to fall freely on monolithic glass and induce a random surface flaw population. 390 annealed glass specimens grouped in 26 series were artificially aged using different combinations of ageing parameters. The specimens were subsequently subjected to destructive and non-destructive testing to determine the influence of each ageing parameter and to establish a combination that produces strength characteristics similar to those of naturally aged glass. Existing artificial ageing recommendations were found to significantly overestimate design strengths by up to 253% at low probabilities of failure, $P_f = 0.008$ and are therefore, deemed unsafe. However, it was found that the falling abrasive method using a different combination of ageing parameters provides good correlation to the strength of naturally aged glass.

1. Introduction

The strength of glass is highly dependent on the condition of its surface. The intrinsic strength of glass is very high and can reach 32 GPa based on the intermolecular bonds that are developed in the glass molecular network [1]. Stress-raising flaws (known as Griffith flaws) accumulate on the glass surface as a result of manufacturing, transportation and surface damage during its service life. This leads to a significant reduction in tensile strength to a value commonly referred to as the extrinsic strength (Eq. (1)).

$$\sigma_f = \frac{K_{IC}}{Y \cdot \sqrt{\pi \cdot a}} \quad (1)$$

where Y: geometry factor (depending on the shape of the crack), α: crack depth and K_{IC}: fracture toughness.

For example, for a typical half penny shaped crack with $a = 50$ μm on the surface of the glass and $K_{IC} = 0.75$ MPa m$^{0.5}$ and $Y = 0.713$, the extrinsic strength of glass is reduced to $\sigma_f = 76.7$ MPa (Eq. (1)). Therefore, a 99.8% reduction is noticed between intrinsic and extrinsic strength.

Damage that accumulates during the service life of glass is a result of natural ageing caused by contact, abrasion or impact and typically depends on the level of exposure. Previous research found a reduction of 35–85% in extrinsic strength with respect to the extrinsic strength of as-received annealed glass [2–5]. Therefore, knowledge of the long term mechanical performance of glass is essential when designing with glass. However, only a few studies are available on the strength of weathered annealed glass [2–7] and even fewer on the strength of weathered toughened glass

* Corresponding author.
E-mail address: kd365@cam.ac.uk (K.C. Datsiou).

http://dx.doi.org/10.1016/j.conbuildmat.2017.03.094
0950-0618/

[8]. Frequently, research on the durability of glass components focuses on the response of the interlayer in laminated glass and its viscoelastic response to load duration and environmental conditions in order to investigate the monolithic/layered response of the laminated glass component [9–12]. However, the mechanical durability of the glass itself can be divided into erosive resistance and scratch resistance.

The erosion of glass occurs when glass is exposed to flying projectiles that repeatedly impact its surface (e.g. a glass panel in a façade) and lead to material removal. The risk increases in cases of extreme wind and locations where windstorms are common. The most common types of flying projectiles in urban areas are roof gravel, roof tiles and timber [13]. Sand abrasion is used for the evaluation of the erosive resistance of glass. This can either be achieved by: (a) a sand trickling set-up ([5,14–18]) where sand is allowed to fall freely from a controlled height onto the surface of the glass or; (b) sandblasting ([19–22])) i.e. propelling of sand by compressed air towards the surface of the glass. The erosive resistance of the glass is a function of the particle size, impact velocity, duration of abrasion and mass of abrasive medium [22]. Damage increases with higher quantities of abrasive, impact angles and speed of impact. However, the erosive resistance in these studies is mainly evaluated by means of non-destructive tests (roughness characterisation, optical transmission and mass loss), thereby disregarding glass strength. Basic strength data are shown in [15], [16], however, a comprehensive statistical analysis of glass strength is only available in [5] reporting a 59% reduction in as-received characteristic strength ($P_f = 0.05$) after sand-abrasion with 6 kg of sand dropped from a height of 1 m. However, further experimental testing and a subsequent detailed statistical analysis on glass strength due to erosive ageing mechanisms is needed to determine the influence of the artificial ageing parameters during the sand abrasion and their correlation to naturally induced damage.

Glass elements are also vulnerable to scratches when objects of higher hardness are forced into the glass and dragged along its surface. Scratches can be induced due to mishandling of the glass during transportation/installation processes, cleaning and in-service conditions. Scratch resistance is typically evaluated with indenters and commercially available scratching devices that can accommodate geometrically different indenter tips [23–25]. Depending on the level of damage and their configuration, scratches can be described with one of the following regimes [26]: (a) *micro-ductile*: permanent deformation and potential lateral cracks (Fig. 1) are induced in the glass.; (b) *micro-cracking*: radial/median cracks (Fig. 1) are formed while lateral cracks extend and intersect with the surface; (c) *micro-abrasive*: radial and median cracks are also formed in this regime while the intersection of the lateral cracks with the surface is continuous along the length of the scratch and accompanied by material removal, known as chips (debris, Fig. 1).

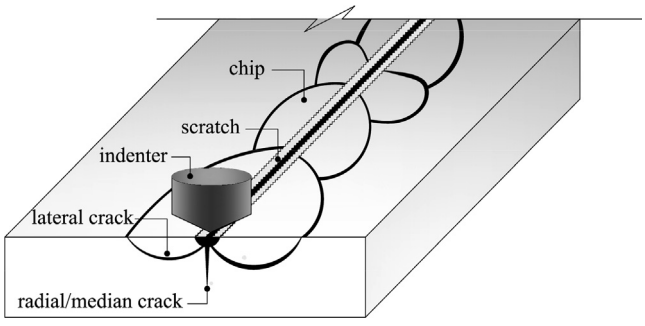

Fig. 1. Morphology and types of cracks.

The scratch resistance of glass and the associated regimes depend on the geometry of the indenter, the chemical composition of the glass, the environmental conditions and the curing time of the scratch, and the scratching speed ([23–27]). Scratches in the micro-ductile regime are more likely to form in glasses with higher silica content. Sharp indenters (e.g. 60°) also result in scratches in the micro-ductile regime while realistic scratches approximating those induced during cleaning (micro-cracking regime) are induced with 90° or 120° conical indenters. Strength recovery after scratching, known as crack healing, was found to occur particularly during the first 24 h of curing time after inducing flaws on the glass surface. The crack healing led to an increase in mean strength of 32% and 42% for curing at ambient conditions (RH = 50%) and curing under water, respectively [27].

Despite the existing research on erosive and scratch mechanisms of glass, a comprehensive and reliable method for the artificial ageing of glass has yet to be established. The selection of a suitable artificial ageing method should depend on the level of exposure/type of application where the glass is to be installed and correspondingly on the expected type of critical flaw (i.e. caused by scratching or erosion). In fact, it was shown that different ageing methods were preferred for two different sources of naturally aged glass, exposed mainly to linear scratching and erosive action, respectively [18,27]. In particular, the induction of scratches is preferred in [27] over other abrasion methods; scratches were found to be a better optical match, based on dye penetrant inspection used to reveal flaws in the naturally aged glass of that study and additionally, artificial ageing with sand abrasion was difficult to reproduce [27]. Whereas glass artificially aged by sand trickling was found to be more representative of the surface roughness and strength of a different source of naturally aged glass exposed to erosive action, than scratched glass [18].

DIN 52348 [28] (similar to ASTM D968-05 for organic coatings [29]) is the only available standard for glass ageing investigations. This standard proposes a sand trickling test for the artificial ageing of glass and the evaluation of its durability. However, DIN 52348 and similarly ASTM D968-05 have some important limitations, namely: (a) there is no published research on the basis of the sand trickling parameters proposed in the standard; (b) there is no published research on the correlation between damage induced artificially and the damage generated by natural phenomena; and; (c) the durability of glass is evaluated in terms of light transmission and the magnitude and scatter of the resulting strength data is disregarded.

This study focuses on applications where erosive ageing on annealed glass is more likely to occur than scratching. In particular, it investigates whether the falling abrasive (also known as sand trickling or dropped grit) method can be used to replicate the strength characteristics of naturally aged glass. The main objective is to identify an optimal combination of artificial ageing parameters that if applied on annealed glass would induce similar levels of damage to those of naturally aged glass. This combination of artificial ageing parameters would therefore, provide a quick and reliable means of assessing the long term performance of novel glass compositions and treatments. Details on the specimens, the falling abrasive method and the non-destructive and destructive evaluation tests (optical microscopy and coaxial double ring tests) used in this study are provided in Section 2. The salient results for the naturally and artificially aged glass are presented in Section 3 including the influence of each artificial ageing parameter on the strength of glass and its correlation to the strength of naturally aged glass. Finally, salient conclusions are found in Section 4.

2. Specimens and methods

2.1. Specimens

Monolithic annealed soda–lime–silica glass (AN) in the form of naturally aged (NA-AN) and un-aged as-received glass (AR-AN) was used to investigate the effectiveness of the falling abrasive method for the artificial ageing of glass. The naturally aged glass was used as a reference for the artificially aged series (SA). Naturally aged glass was obtained from a building that was exposed to natural ageing mechanisms for 20 years as part of a façade in Norfolk, UK. This was a low rise building in a rural location with a distance greater than 10 km from the coast. The glass was cleaned with warm soapy water to remove the organic residue that had accumulated on its surface during its in-service life and was then cut to size with a diamond cutter. Two series of NA-AN ($NA\text{-}AN_a$ & $NA\text{-}AN_b$) were tested; specimens for these series were obtained from the same façade but different panels. AR-AN is new as-received annealed glass, obtained from a single supplier and cut to size by the supplier. One series of this glass was tested in its as-received state (AR-AN) while the rest were subjected to sand abrasion with the falling abrasive method (SA-AN).

Table 1 summarizes the types of glass and the number of specimens used in this study. The chemical composition of the naturally aged and the as-received glass used in this study was found to be similar (as reported in [3]). The surface residual stress of the naturally aged and the as-received glass was also found to be similar. This was measured through the thickness of the glass with a scattered light polariscope (SCALP-05, GlasStress Ltd. [30]). The surface compression for the naturally aged and the as-received annealed glass was 3.7 ± 1.0 MPa and 2.31 ± 0.65 MPa, respectively.

2.2. Experimental methods

The artificial ageing method and the evaluation tests used in this study are described in turn in this section. Experimental tests were always performed on the weaker surface of the specimens; for the naturally aged glass this is the "external" surface i.e. the surface that was exposed to weathering action during its service life and for the as-received annealed glass the tin side (identified with a UV-light). It was not possible to distinguish between tin side and air side of the naturally aged glass, because unlike the as-received glass, the reflection of the two surfaces on exposure to UV light was indistinguishable. However, this is not expected to affect the results as the critical flaw depths found in naturally aged glass as a result of natural weathering (micrographs shown in Section 3.1), are larger than those induced on the tin side during the float process (≈28.9 μm [31]).

2.2.1. Artificial ageing with falling abrasive

The as-received glass (AR) was artificially aged with the falling abrasive method (Fig. 2a). This method is intended to induce a random flaw population on the surface of the glass and is based on the methods proposed in DIN 52348 [28] and ASTM D968-05 [29]. The artificial ageing procedure was performed as follows:

i. The abrasive medium is loaded in a sand container. Silica sand and riverside gravel (Fig. 3a-b) with different grain sizes ranging between $0.5 \leq GSR \leq 1.0$ mm and $1.0 \leq GSR \leq 9.5$ mm respectively were used in this study (grain size curves are shown in Appendix A) The morphology of the silica sand is mostly rounded with few angular edges while riverside gravel is rounded with smooth edges (Fig. 3a-b);

Table 1
Specimen overview.

Abbr.	Glass type	Ageing	Dimensions	Nominal thickness	No. of series	Specimens/series
NA-AN	Float SLS annealed	Natural	150 × 150 mmm	2.83 ± 0.08 mm	2	15
AR-AN	Float SLS annealed	As-received	150 × 150 mm	2.85 ± 0.03 mm	1	15
SA-AN	Float SLS annealed	Sand abraded	150 × 150 mm	2.85 ± 0.04 mm	26	15

*SLS: soda lime silica.

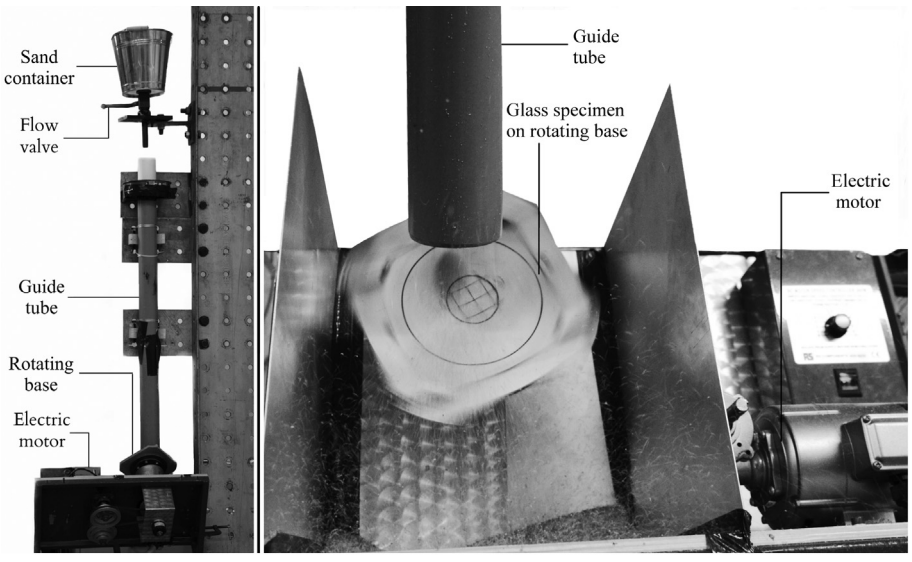

Fig. 2. Falling abrasive test: (a) Set-up (rear view) and; (b) Rotating specimen base (front view).

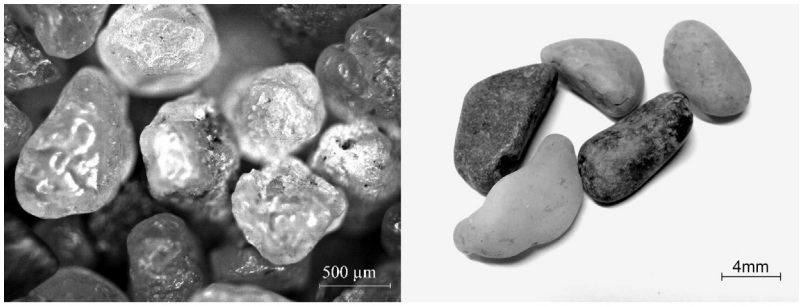

(a) (b)

Fig. 3. Morphology of: (a) silica sand grains ($0.5 \leq GSR \leq 0.7$ mm) and; (b) riverside gravel ($8.0 \leq GSR \leq 9.5$ mm).

ii. The specimen is clamped to a steel base with the tin side facing upwards. This is the side that will be subjected to artificially ageing. The base is inclined at an angle of 45° to the ground and rotates with the aid of an electrical motor (Fig. 2b);
iii. As the specimen rotates at full speed, the abrasive material is allowed to trickle onto the surface of the glass under the effect of its gravity. The rate of the abrasive flow is controlled with a manually operated steel valve that is fitted below the sand container; when the valve is fully open the flow rate is 100 g/s; a guide tube (ø82 mm) prevents the abrasive material from dispersing over a wide area as it falls.
iv. The artificial ageing process ends when the whole mass of the abrasive material impacts the surface of the specimen.

Table 2
Range of artificial ageing parameters.

Parameter	Abbr.		Values investigated
Drop Height	H	(m)	3.0, 2.3, 1.65, 1.2
Abrasive medium			Silica sand & river gravel
Mass of abrasive	m	(kg)	1.0, 1.5, 2.0, 3.0, 4.0, 5.0
Maximum grain size range	MGS	(mm)	0.7, 1.0, 5.6, 9.5
Gravel%	p		0, 0.1, 10
Rotation rate	RR	(rpm)	0, 125, 250
Curing time	t_c	(h)	2, 168
Environmental conditions during curing			Ambient, under water

Table 2 summarizes the different values for artificial ageing parameters (drop height, rotation rate of the base, mass and grain size range of abrasive material) that were tested in this study for the sand abraded series (SA).

2.2.2. Optical microscopy and coaxial double ring tests

Qualitative micrographs of the surface of the glass specimens were obtained with a Leica LG optical microscope. Prior to the destructive testing, a clear self-adhesive film was applied, to the non-aged surface of the specimen to allow post-testing fractography. Destructive testing was performed approximately 2 h after the artificial ageing, in a coaxial double ring set-up (CDR, Fig. 4a). The diameters of the loading and the reaction ring are $D_L = 51$ and $D_R = 127$ mm, respectively (Fig. 4b) and comply with ASTM C1499-03 [32]. The loading ring was connected to a 2 kN load cell Instron machine with an articulated joint to ensure uniform contact between the loading ring and the surface of the specimen. The specimens were oriented so that the tin side of the as-received annealed glass specimens and the external side of the naturally aged glass specimens were in tension during the destructive testing and the self-adhesive film was on the compressive surface. A displacement rate of 13.6 mm/min (corresponding to a stress rate of 20 MPa/s within the loading ring region) was chosen in order to cause fracture within 1–7 s thereby minimizing the influence of sub-critical crack growth (quasi-inert conditions).

The self-adhesive film was successful in holding the fragments together after fracture of the specimen. This enabled fractographic analysis as follows: (i) the fracture pattern of the whole specimen was carefully observed to identify the origin of the critical flaw

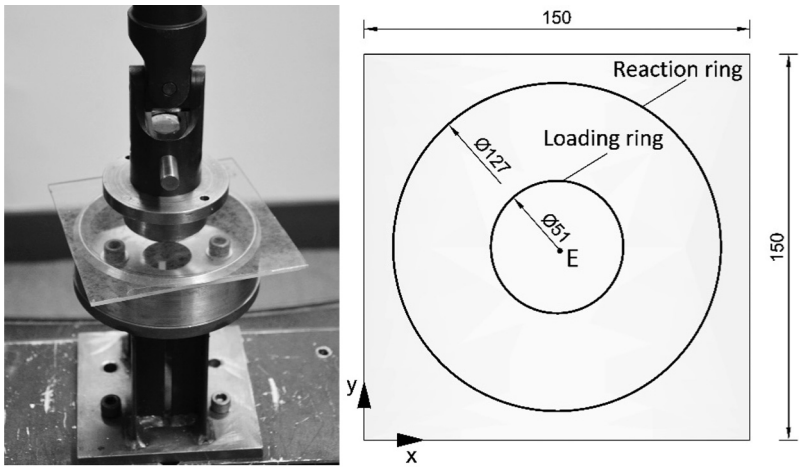

(a) (b)

Fig. 4. (a) Coaxial double ring set-up; (b) Top view of specimen.

(Fig. 5a). Specimens with origins of failure located outside the loading ring were excluded from further analysis of glass strength; (ii) the fragment, containing the critical flaw, was removed carefully to avoid inducing additional flaws on the cross-section of the glass; (iii) the fragment was cut to size, if needed, with a diamond glass cutter to fit under an optical microscope; (iv) the lateral face of the fragment containing the critical flaw was investigated under an optical microscope. Wallner lines pointed towards the direction of the critical flaw while the mirror, mist and hackle (Fig. 5b) revealed its location (Fig. 5c) [33].

2.3. Data processing methods

2.3.1. Failure load to failure stress

To assist the experimental testing two FEA models (Fig. 6) were constructed in Abaqus – Dassault Systèmes v6.12 [34] to simulate the destructive testing (CDR) of the glass (Poisson's ratio $\upsilon = 0.23$ and Young's modulus $E = 70$ GPa). Each of them consisted of 6774 quadratic quadrilateral shell elements (S8R). The first model considered friction between the loading/reaction ring and the glass specimen while the other neglected it. Experimental strain gauge data of the tension surface of the glass showed that the full friction FEA model was more representative than the null-friction model. Additionally, the full friction model was found to be more accurate than the analytical formula of Eq. (2) (ASTM C1499-03 [32] based on Timoshenko plate theory) for loads and centre displacements exceeding 700 N and 0.55 mm respectively when non-linear (membrane) effects start to become significant (Fig. 6b). Therefore, the full friction model was used to derive failure stress in this study.

$$\sigma_{f,60\,\mathrm{sec}} = \frac{3 \cdot P}{2 \cdot \pi \cdot t^2} \cdot \left[(1-\nu) \cdot \frac{D_R^2 - D_L^2}{2 \cdot D^2} + (1+\nu) \cdot \ln\left(\frac{D_R}{D_L}\right) \right] \tag{2}$$

where: P: the failure load, t: the thickness of the specimen, D_R and D_L: the diameters of the reaction and the loading ring respectively, $\nu = 0.23$: Poisson's ratio and

$$D = \frac{l}{0.90961 + 0.12652\frac{t}{D_R} + 0.00168 \cdot \ln\left(\frac{l-D_R}{t}\right)} \tag{2a}$$

and

$$l = 0.5 \cdot (l_x + l_y) \tag{2b}$$

2.3.2. Failure stress to equivalent failure stress

Time-to-failure, t_f, varied from specimen to specimen. Therefore, to normalize sub-critical crack growth effects, the experimental stress history was converted to a uniform equivalent stress history that causes the same level of crack growth. In particular, the ramp stress history induced during the experiments was transformed with Eq. (3) to an equivalent uniform stress, $\sigma_{f,60}$, for a reference time period, t_{ref}, of 60 s.

$$\int_0^{t_f} \left(\frac{\sigma_f \cdot t}{t_f}\right)^n dt = \int_0^{t_{ref}} \sigma_{f,60}^n dt \Rightarrow \sigma_{f,60} = \sigma_f \cdot \left[\frac{t_f}{t_{ref} \cdot (n+1)}\right]^{1/n} \tag{3}$$

where σ_f: the failure stress and n: the exponential crack velocity parameter also known as static fatigue constant ($n = 16$ in this study [1]).

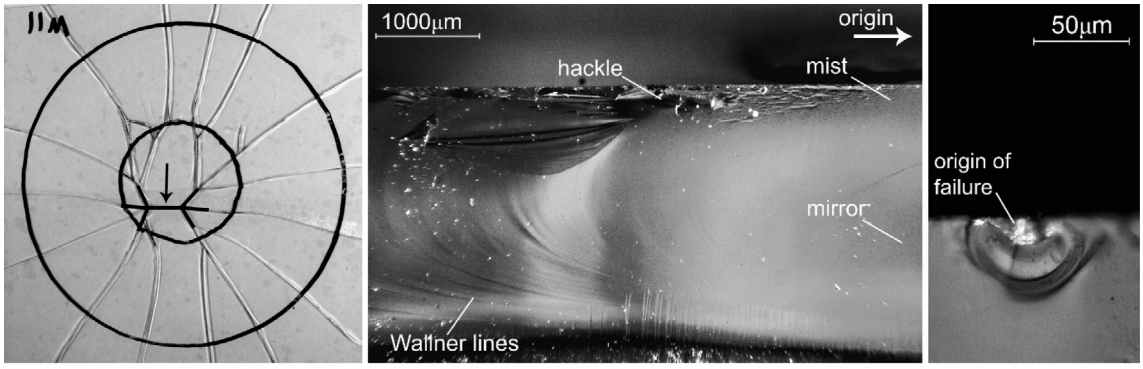

Fig. 5. (a) Approximate location of the origin of failure; (b) Mirror, mist and hackle and (c) critical flaw.

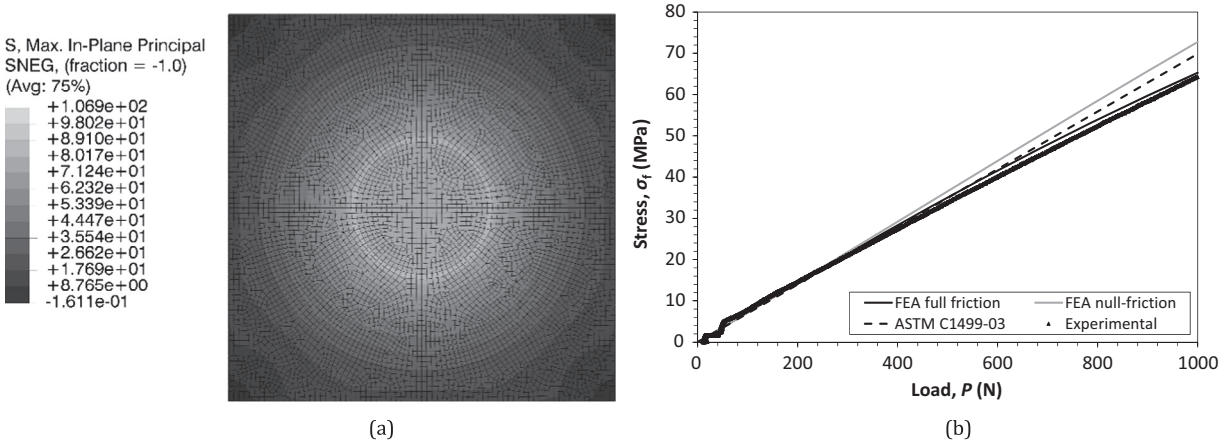

Fig. 6. Max principal stress of tension surface: (a) FEA ($P = 1500$ N) and; (b) exp., num. and anal. data at point E (Fig. 4b).

2.3.3. Statistical analysis

A Weibull distribution was fitted to the experimental equivalent strength data [35]. The cumulative distribution function (CDF) of the Weibull distribution is described by:

$$P_f(\sigma_{f,60}) = 1 - \exp\left[-\left(\frac{\sigma_{f,60}}{\theta}\right)^{\beta}\right] \quad (4)$$

where P_f: the probability of failure, β: the shape parameter and θ: the scale parameter

The CDF can be linearized (Eq. (5)) in the form of $y = bx + c$ by taking the logarithm of each side twice:

$$\ln\left(\ln\left(\frac{1}{1-P_f}\right)\right) = \beta \cdot \ln \sigma_{f,60} - \beta \cdot \ln \theta \quad (5)$$

where $y = \ln\left(\ln\left(\frac{1}{1-P_f}\right)\right)$ and $x = \ln \sigma_{f,60}$. Consequently, the gradient of the CDF depends on the shape parameter ($b = \beta$) while the intercept is $c = -\beta \cdot \ln\theta$.

2.3.4. Weibull parameter estimation

A linear regression method was used in this study to determine salient Weibull characteristics. Equivalent strength data are initially ranked in ascending order ($i = 1$ to n). Subsequently, estimators, G_i, are used to assign a probability of failure (in cumulative form) by applying equal weights to each data point and define their plotting position $\left(\ln \sigma_{f,60}, \ln\left(\ln\left(\frac{1}{1-G_i}\right)\right)\right)$. The simplest forms for estimators are: $G = i/n$ and $G = (i\text{-}1)/n$. However, these estimators would eliminate the highest/lowest data points from consideration/plot and are generally avoided in Weibull statistics. Hazen's estimator (Eq. (6)) was therefore, proposed to provide an intermediate solution between these two estimators by dividing the jump between them.

$$G_i = \frac{i - 0.5}{n} \quad (6)$$

However, estimators apply equal weights to each data point without taking into account the uncertainty of y_i or G_i. To account for these uncertainties weight functions can be introduced in the regression method leading to a weighted least squares approach [36,37]. Additionally, if one considers that glass strength data can be successfully described by a 2-parameter Weibull distribution [35,38], the weighted least squares approach is more accurate for small sized samples [39] in terms of goodness of fit and erring on the side of caution when compared to the Good Linear Unbiased Estimators approach proposed in EN 12603 [40].

Faucher & Tyson's weight function (Eq. (8)) alongside Hazen's estimator are used in this study as they were found to produce better goodness of fit when compared to other weight functions and estimators [39]. The Weibull parameters were therefore, computed in this study with Eqs. (7a) & (7b) and Eq. (8):

$$\beta = \frac{\sum_{i=1}^{n} W_i \cdot \sum_{i=1}^{n} (\ln \sigma_i \cdot y_i \cdot W_i) - \sum_{i=1}^{n} (\ln \sigma_i \cdot W_i) \cdot \sum_{i=1}^{n} (y_i \cdot W_i)}{\sum_{i=1}^{n} W_i \cdot \sum_{i=1}^{n} ((\ln \sigma_i)^2 \cdot W_i) - \left(\sum_{i=1}^{n} \ln \sigma_i \cdot W_i\right)^2} \quad (7a)$$

$$-\beta \cdot \ln \theta = \frac{\sum_{i=1}^{n} (y_i \cdot W_i) - \beta \cdot \sum_{i=1}^{n} (\ln \sigma_i \cdot W_i)}{\sum_{i=1}^{n} W_i} \quad (7b)$$

$$W_i = 3.3 \cdot G_i - 27.5 \cdot [1 - (1 - G_i)^{0.025}] \quad (8)$$

where W_i: the weight for each data point.

The resulting distribution was then evaluated using the Anderson Darling goodness of fit, p_{AD}, considering a 5% confidence level.

Strength data were subsequently evaluated for the design and mean probabilities of failure i.e. $P_f = 0.008$ and $P_f = 0.50$, respectively. A probability of failure of 0.008 for the design strength follows the recommendations of ASTM E1300-09 [41], but any other suitably low probability of failure could be selected for comparing across the tests performed in this study. Additionally, confidence intervals were estimated following the procedure in EN 12603 [40] to determine whether the number of specimens were sufficient for the artificially aged series (refer to Appendix B).

3. Results and discussion

3.1. Microscopy

Micrographs of the surfaces of as-received, naturally aged and sand abraded glass are shown in Fig. 7. As-received annealed glass is almost defect free at a magnification level of 100× (Fig. 7c). However, the surface of the naturally aged glass (Fig. 7a-b) shows signs of moderate to extensive surface flaws. NA-AN_a (Fig. 7a) is more severely aged (mostly digs and some scratches [42]) compared to NA-NA_b (digs, Fig. 7b). Micrographs of the SA series (Fig. 7d-f) show that the damage regime depends on the maximum grain size (*MGS*) of the abrasive medium; micro-ductile and occasionally micro-cracking regimes are noted when the abrasive medium is silica sand ($0.5 \leq GSR \leq 0.7$ mm, Fig. 7d). However, as the *MGS* increases beyond 5.6 mm and riverside gravel are also included in the medium, the flaw size also increases (Fig. 7e-f). The damage in these cases belongs to the micro-cracking or the micro-abrasive regime as the lateral cracks caused by the impact, extend to the surface and in some cases create debris.

Two types of critical flaws were distinguished for naturally aged glass as was expected based on §1: (a) pits induced by impact potentially by flying projectiles or objects forced on the surface of glass during its service life of the glass or; (b) scratches potentially induced during transportation, installation and/or cleaning of the glass (Fig. 8a-b). The size of the critical flaws in sand abraded series is proportional to the *MGS* of the abrasive medium (Fig. 8c-f). Additionally, the formation of radial/median cracks depends on the type of the abrasive medium; radial/median cracks were typically induced when gravel is included in the abrasive medium. However, radial/median cracks were rarely found when only silica sand is used (micro-ductile regime in Fig. 8c and micro-cracking regime in Fig. 8d).

3.2. Fracture strength of as-received and naturally aged annealed glass

The differences in size and quantity of the flaws observed on NA-AN_a and NA-AN_b discussed in §3.1 on naturally aged glass are also evident in the fracture strength of the respective glass specimens (Table 3, Fig. 9); The design ($P_f = 0.008$) and mean ($P_f = 0.50$) strengths of NA-AN_a were 46% and 29% lower than NA-AN_b. A reduction in fracture strength was expected as the surface damage on the NA-NA_a glass was more extensive. More importantly, naturally aged glass suffered 73–85% and 51–66% reduction in design and mean strength ($\Delta\sigma_{NA,AR}/\sigma_{NA}$%) respectively with respect to as-received glass.

3.3. Fracture strength of sand abraded series

DIN 52348 [28] prescribes a drop height $H = 1.65$ m, a mass of abrasive medium $m = 3.0$ kg, a grain size range $0.5 \leq GSR \leq 0.7$ mm and a rotation rate of the base $RR = 250$ rpm. The failure stress data of the sand abraded series using these artificial ageing parameters (SA2) produce a good correlation with the mean strength ($P_f = 0.50$) of naturally aged glass (Fig. 9). However, the results significantly overestimate strengths at low probabilities of failure;

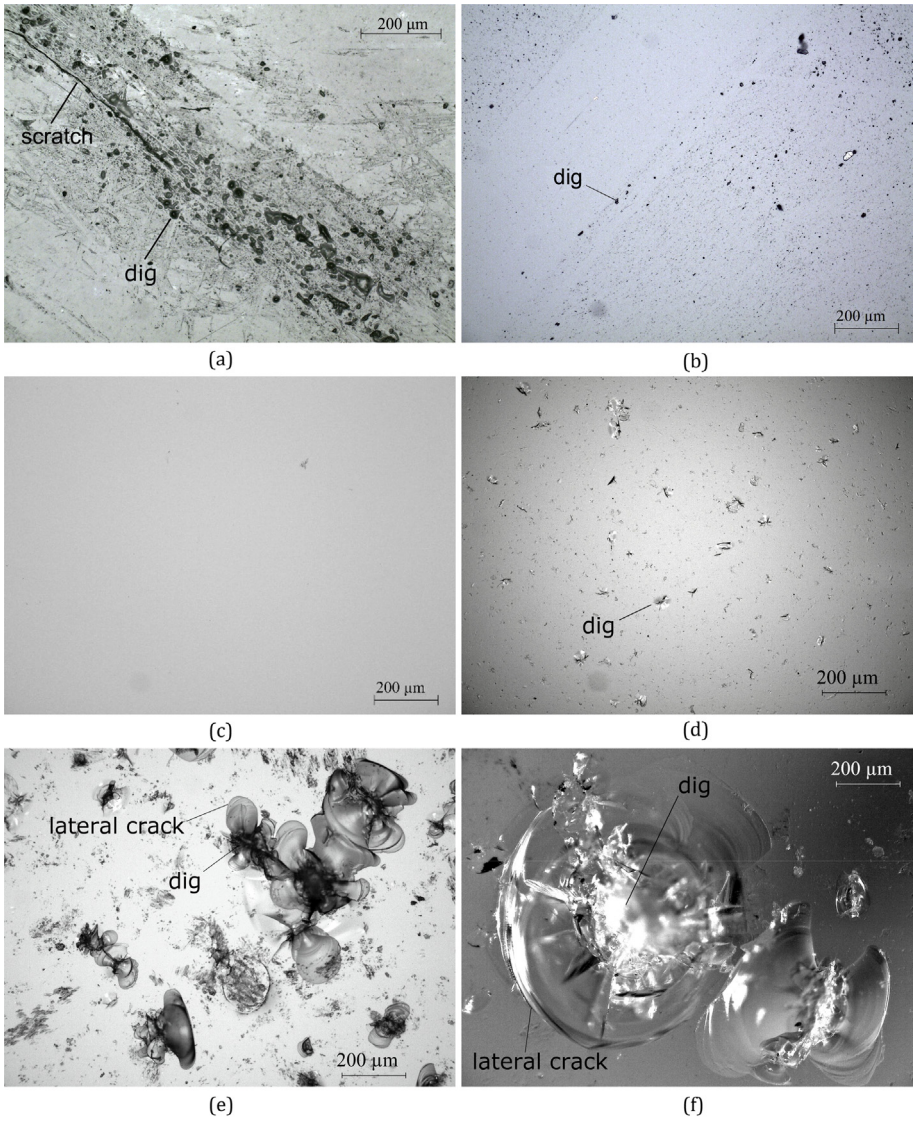

Fig. 7. Micrographs of the surface of: (a) NA-AN$_a$; (b) NA-AN$_b$; (c) AR-AN; (d) SA4 ($0.5 \leq GSR \leq 0.7$ mm); (e) SA17 ($0.5 \leq GSR \leq 5.6$ mm) and; (f) SA23 ($0.5 \leq GSR \leq 9.5$ mm).

$92 \leq \Delta\sigma_{SA,NA}/\sigma_{NA} \leq 253\%$ overestimation of strength was found for $P_f = 0.008$ (Table 3). Therefore, DIN 52348 [28] does not reproduce surface damage that is representative of the natural ageing processes that the glass of this study underwent during its service life.

Therefore, it is pertinent to identify a combination of artificial ageing parameters that would produce a representative cumulative distribution function to the ones reported for naturally aged glass. For this reason, the influence of each artificial ageing parameter (drop height (H), mass (m), maximum grain size (MGS), gravel percentage (p), rotation rate (RR) and curing time (t_c)) on the strength of the sand abraded glass is discussed in turn in this section.

3.3.1. Drop height influence

Drop heights, H, of 1.2 m, 1.65 m (prescribed in DIN 52348 [28]), 2.3 m and 3.0 m were considered to investigate the influence of the drop height on the strength of the artificially aged glass. All other artificial ageing parameters were kept constant at $m = 3$ kg, $0.5 \leq GSR \leq 0.7$ mm, $RR = 250$ rpm and $t_c = 2$ h. Fig. 10 shows that strength reduces as the drop height increases.

3.3.2. Mass of abrasive medium influence

Masses of abrasive medium of 1.0, 1.5, 2.0, 3.0 (prescribed in DIN 52348 [28]), 4.0 and 5.0 kg were tested individually to investigate their influence on glass strength. All other artificial ageing parameters were kept constant at $H = 3.0$ m, $0.5 \leq GSR \leq 0.7$ mm, $RR = 250$ rpm and $t_c = 2$ h.

The results show that the failure mode of the artificially aged glass depends on the mass of the abrasive medium; unimodal Weibull distributions were found for masses ≥ 3.0 kg (Fig. 11a) and bi-modal Weibull distributions were found for masses <3.0 kg (Fig. 11b). A bi-modal Weibull distribution signifies that the fracture data can be divided in two groups and it suggests that the critical flaws on either side of the bi-modal discontinuity are morphologically different.

3.3.2.1. $m \geq 3.0$ kg. The increase in the mass of the abrasive medium did not result, in the expected decrease in strength (Fig. 11a). As the mass increased above 3 kg, the strength of the specimens also increased at low probabilities of failure and converged at very high probabilities of failure. This increase in strength can potentially be attributed to the extended sand abrasion; as the mass of the abrasive medium increases material can be uniformly removed from the surface reducing the overall thickness of the glass and smoothing out flaws induced by the sand abrasion. The depth of the flaws is thereby reduced making the flaws less severe.

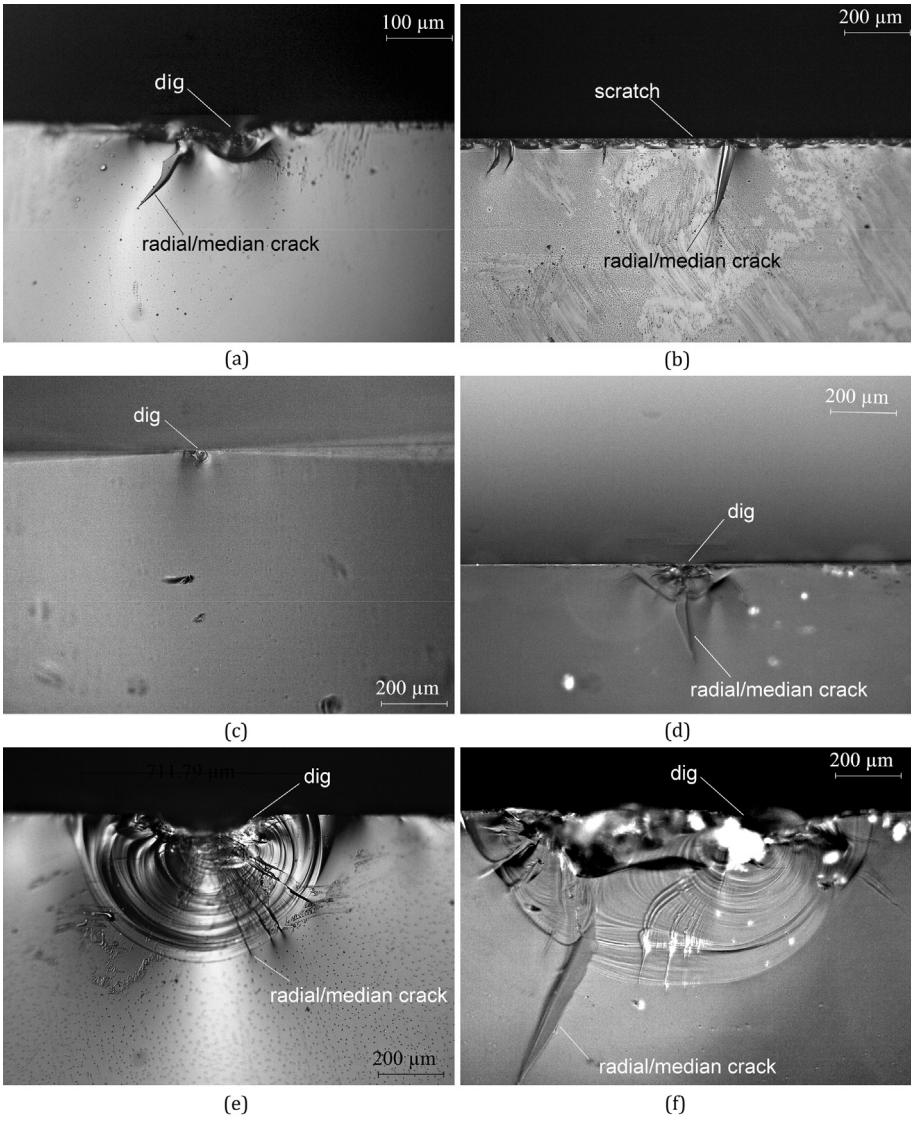

Fig. 8. Critical flaws found in: (a-b) NA glass; (c) SA glass for *MGS* = 0.7 mm; (d) SA glass for *MGS* = 0.7 mm; (e) SA glass for *MGS* = 5.6 mm and; (f) SA glass for *MGS* = 9.5 mm.

3.3.2.2. m < 3.0 kg. Unsurprisingly, unimodal Weibull distributions commonly used in glass strength statistics [40], provided a poor fit ($p_{AD} < 0.05$) to the bi-modal data from the experiments; these series can therefore, be more accurately described by mixed Weibull distributions (Eq. C1, refer to Appendix C) providing acceptable goodness of fit.

However, post-fracture optical microscopy revealed that the critical flaws belonging to the first mode of the distribution i.e. data points corresponding to lower failure stresses, originate from linear scratches of different morphology (Fig. 12b) that are morphologically different from the flaws induced by the sand impact (second mode of the distribution, Fig. 12b). These linear scratches were potentially introduced during transportation and handling of the glass. The flaw depth of these linear scratches was larger than the depth of flaws introduced by the artificial ageing (Fig. 12a-b) and were therefore, critical. The mixed Weibull distribution is therefore, not used further in this study since pre-existing flaws and the uncertainties associated with their formation, are excluded from the analysis of the artificial ageing parameters. In fact, unimodal failures with acceptable goodness of fit can be achieved for masses < 3 kg when the data points that correspond to the first mode of failure (scratches) are excluded (Table 3). In general, masses < 3.0 kg should be avoided in order to eliminate the influence of flaws created during handling and transportation of the glass.

3.3.3. Maximum grain size of the abrasive medium

Well graded ranges of abrasive medium, namely $0.5 \leq GSR \leq 0.7$ mm, $0.5 \leq GSR \leq 1.0$ mm, $0.5 \leq GSR \leq 5.6$ mm and $0.5 \leq GSR \leq 9.5$ mm (grain size distribution curves shown in Appendix A, Fig. A1a), were used to study the influence of the maximum grain size, *MGS*, on the strength of the artificially aged glass while all other artificial ageing parameters were kept constant at $H = 3.0$ m, $m = 3$ kg, $RR = 250$ rpm and $t_c = 2$ h. A small increase in *MGS* from 0.7 to 1.0 mm produces negligible differences in strength (7% and 3% increase for *MGS* = 0.7 mm for the design and mean strength respectively with respect to *MGS* = 1.0 mm, Fig. 13). However, significant strength reduction was noted when the maximum grain size increased considerably (44% & 46% reduction in design & mean strength for *MGS* = 5.6 mm and 59% & 57% reduction in design & mean strength for *MGS* = 9.5 mm).

Table 3
Salient results of the Weibull statistics analysis for fracture strength data of all series.

Series	Artificial ageing parameters						Weibull parameters				Fractile values			
	H m	m kg	GSR mm	p %	RR rpm	t_c h	β	θ MPa	p_{AD} %	CV %	$\sigma_{f,0.008}$ MPa	max σ MPa	min σ MPa	$\sigma_{f,0.5}$ MPa
NA-ANa	–	–	–	–	–	–	3.39	41.68	9.69	32.58	10.00	61.06	24.12	37.41
NA-ANb	–	–	–	–	–	–	4.22	57.54	79.58	26.70	18.36	75.80	29.41	52.76
AR-AN	–	–	–	–	–	–	9.36	112.92	66.63	12.81	67.44	129.67	93.243	108.58
SA1	1.20	3.0	0.5–0.7	0*	250	2	34.66	47.24	48.86	3.63	41.10	49.11	44.61	46.74
SA2	1.65	3.0	0.5–0.7	0*	250	2	19.47	45.20	35.86	6.36	35.28	48.14	40.96	44.36
SA3	2.30	3.0	0.5–0.7	0*	250	2	15.76	41.55	64.12	7.80	30.59	44.25	30.96	40.59
SA4	3.00	3.0	0.5–0.7	0*	250	2	17.29	35.28	72.92	7.13	26.69	37.50	30.38	34.54
SA5	1.20	1.0	0.5–0.7	0*	250	2	14.78	49.28	17.16	8.29	35.56	52.88	38.87	48.08
SA6	1.20	1.5	0.5–0.7	0*	250	2	13.99	48.84	68.62	8.74	34.59	53.58	39.22	47.57
SA7	1.20	2.0	0.5–0.7	0*	250	2	15.32	48.17	78.44	8.01	35.16	51.26	38.54	47.03
SA8	1.65	1.0	0.5–0.7	0*	250	2	20.86	51.30	11.70	5.95	40.70	55.51	44.89	50.41
SA9	1.65	1.5	0.5–0.7	0*	250	2	16.70	47.57	19.35	7.38	35.63	51.61	43.10	46.53
SA10	1.65	2.0	0.5–0.7	0*	250	2	17.69	45.83	71.81	6.98	34.89	48.51	41.21	44.89
SA11	3.00	1.0	0.5–0.7	0*	250	2	22.35	45.52	59.91	5.57	36.68	48.61	39.44	44.78
SA12	3.00	1.5	0.5–0.7	0*	250	2	22.66	38.22	18.87	5.49	30.89	40.11	31.80	37.61
SA13	3.00	2.0	0.5–0.7	0*	250	2	15.13	43.30	50.66	8.11	31.48	45.67	35.72	42.26
SA14	3.00	4.0	0.5–0.7	0*	250	2	18.38	37.43	72.82	6.73	28.79	39.48	33.22	36.69
SA15	3.00	5.0	0.5–0.7	0*	250	2	41.05	38.91	32.41	3.07	34.59	40.61	36.54	38.56
SA16	3.00	3.0	0.5–1.0	0*	250	2	19.93	36.42	56.89	6.22	28.59	38.45	28.54	35.76
SA17	3.00	3.0	0.5–5.6	45*	250	2	21.17	18.87	17.33	5.87	15.02	20.53	16.65	18.54
SA18	3.00	3.0	0.5–0.7 & 8.0–9.5	0.1	250	2	9.94	28.51	79.98	12.10	17.55	32.03	20.12	27.48
SA19	3.00	3.0	0.5–1.0	0*	0	2	16.22	32.25	67.24	7.59	23.96	34.90	26.57	31.53
SA20	3.00	3.0	0.5–1.0	0*	125	2	13.82	33.86	14.81	8.84	25.52	38.48	27.84	32.97
SA21	3.00	3.0	0.5–0.7 & 8.0–9.5	0.1	250	168	6.20	27.63	58.04	18.81	12.68	33.31	16.29	26.05
SA22	3.00	3.0	0.5–9.5	55*	250	2	15.05	15.22	48.23	8.15	11.04	16.10	12.81	14.85
SA23	3.00	3.0	0.5–0.7 & 8.0–9.5	10	250	2	8.44	17.56	57.53	14.11	9.91	20.91	13.02	16.81
SA24	3.00	3.0	0.5–0.7 & 8.0–9.5	10	250	168	11.55	19.75	15.06	10.50	13.01	22.57	16.16	19.13
SA25	3.00	3.0	0.5–0.7 & 8.0–9.5	10	250	168	11.85	19.21	62.33	10.24	12.78	20.97	14.20	18.62
SA26	3.00	3.0	0.5–0.7 & 8.0–9.5	0.05	250	2	11.90	38.26	19.06	10.21	25.51	43.45	28.37	37.07

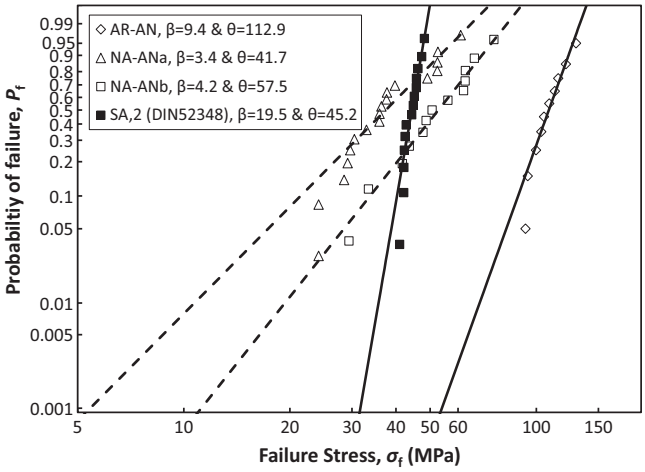

Fig. 9. CDFs for naturally aged (NA), as-received (AR) and SA2 sand abraded (DIN 52348) annealed glass.

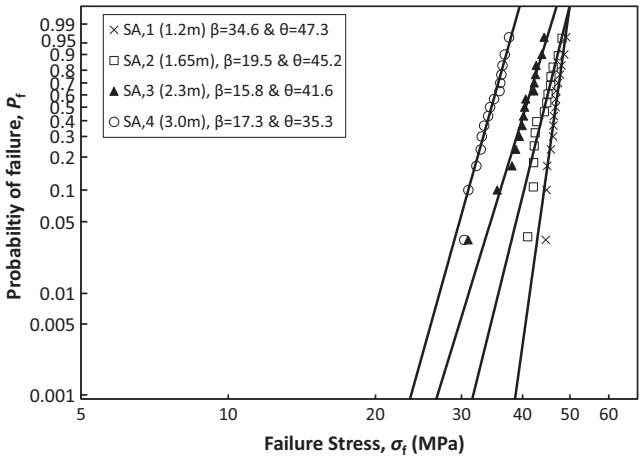

Fig. 10. Effect of drop height on the Weibull distribution plot for $m = 3.0$ kg, $0.5 \leq GSR \leq 0.7$ mm, $RR = 250$ rpm and $t_c = 2$ h.

3.3.4. Percentage of gravel

The influence of the percentage of gravel, p, of the abrasive medium on the strength of glass was also investigated. In particular, abrasive medium of 3 kg was used which predominantly consisted of a grain size range of $0.5 \leq GSR \leq 0.7$ mm and small percentages of gravel ($8.0 \leq GSR \leq 9.5$ mm) namely 0%, 0.05%, 0.1% and 10%. All other artificial ageing parameters were kept constant at $H = 3.0$ m, $m = 3$ kg, $RR = 250$ rpm and $t_c = 2$ h. The integration of a very small percentage of gravel in the abrasive mixture ($p = 0.05\%$ and namely 1 gravel) leads to wider distribution of strength data (Fig. 14, $CV = 10.21\%$ for $p = 0.05\%$ and $CV = 7.13\%$ for $p = 0$, Table 3) seen as a clockwise rotation of the distribution. Increasing the% of gravel further ($p = 0.1\%$ and 10%) leads to the expected strength reduction (Fig. 14) and a clockwise rotation of the distribution similar to $p = 0.05\%$ (CV = 12.10% for p = 0.1% and CV = 14.11% for p = 10%). This clockwise rotation is represented by the decrease in shape factor, β, (Table 3); a reduction of 31%, 43% and 51% was reported for $p = 0.05\%$, 0.1% and 10% respectively with respect to $p = 0\%$. This is an important finding as the shape factor of naturally aged glass is typically low ($3.4 \leq \beta \leq 4.2$ in this study) and therefore, these series are more representative of the naturally aged glass investigated in this study (see §3.1).

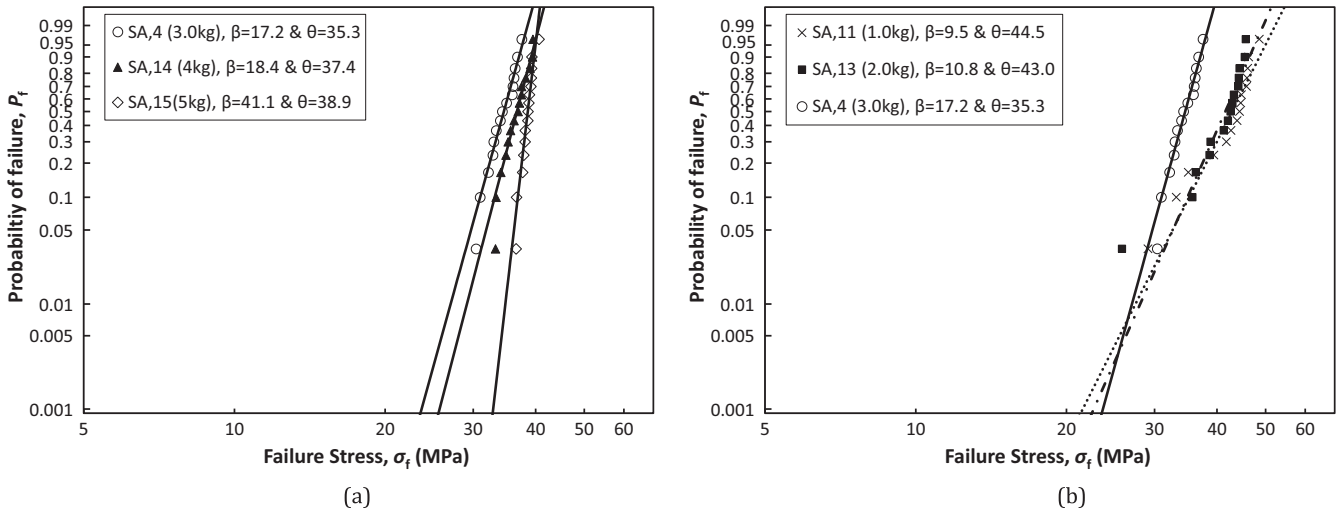

Fig. 11. Effect of mass on the Weibull distribution for H = 3.0 m, $0.5 \leq GSR \leq 0.7$ mm, RR = 250 rpm and t_c = 2 h: (a) $m \geq 3.0$ kg and; (b) $m \leq 3.0$ kg.

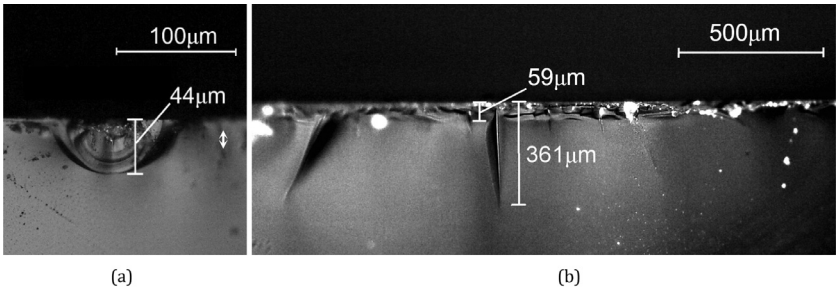

Fig. 12. Critical flaw of: (a) 2nd mode of failure – elliptical flaw created by grain impact and; (b)1st mode of failure- scratch created during handling and transportation.

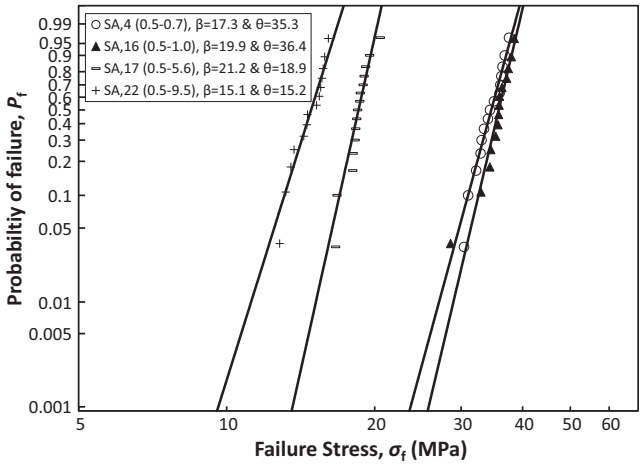

Fig. 13. Effect of maximum grain size on the Weibull distribution plot for H = 3.0 m, m = 3 kg, RR = 250 rpm and t_c = 2 h.

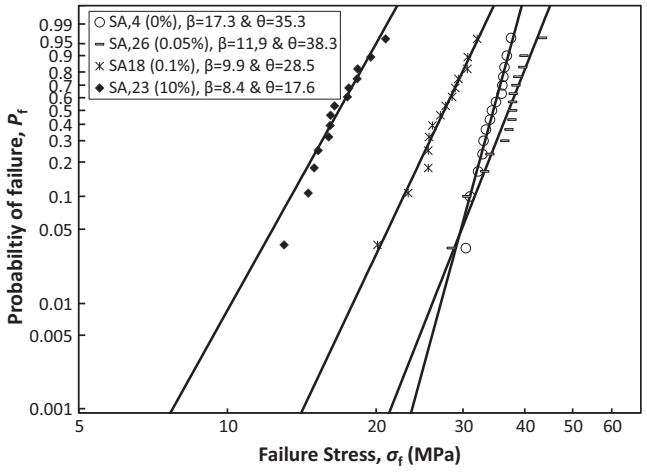

Fig. 14. Effect of the percentage of gravel on the Weibull distribution plot for H = 3.0 m, m = 3 kg, RR = 250 rpm and t_c = 2 h.

3.3.5. Base rotation rate

The effect of the base rotation rate on the strength of the artificially aged glass was investigated for RR = 0, 125 and 250 rpm. All other artificial ageing parameters were kept constant at H = 3.0 m, m = 3.0 kg, $0.5 \leq GSR \leq 1.0$ mm and t_c = 2 h. The results show that increasing the rotation rate leads to an increase in strength (Fig. 15). This is expected because a stationary base results in damage concentration to the confined area directly under the guide pipe, thereby, leading to severer flaws and thus, lower strengths.

3.3.6. Curing time and environmental conditions

The influence of the curing time and environmental conditions during curing were also investigated in this study. Curing time, t_c, is the time period between the artificial ageing process and the CDR tests. Two cases were considered for the curing time: (a) destructive testing immediately after the sand abrasion ($t_c \approx 2$ h)

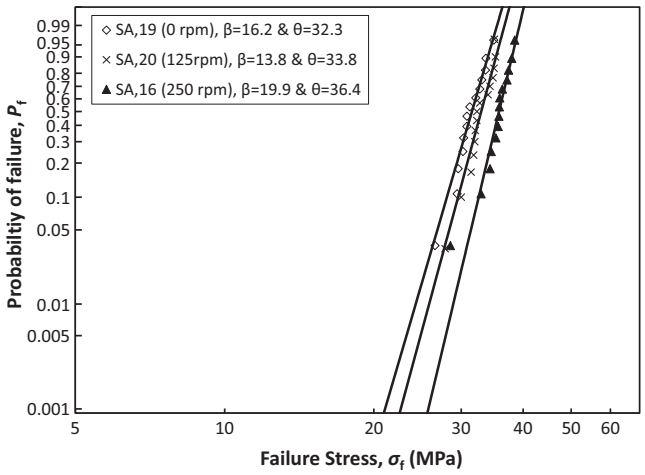

Fig. 15. Effect of rotation rate on the Weibull distribution plot for $H = 3.0$ m, $m = 3$ kg, $0.7 \leq GSR \leq 1.00$ mm and $t_c = 2$ h.

and; (b) destructive testing after storing the sand abraded specimens for 1 week ($t_c \approx 7$ days). Storing conditions involved: (a) ambient lab conditions ($T = 22 \pm 3$ °C and $RH = 42 \pm 8\%$) and; (b) storing under potable tap water.

3.3.6.1. Influence of curing time at ambient conditions. Curing of the artificially aged glass was used in SA21($H = 3.0$ m, $m = 3.0$ kg, $RR = 250$ rpm $0.5 \leq GSR \leq 0.7$ mm (99.9%) & $8.0 \leq GSR \leq 9.5$ mm (0.1%) and $t_c = 2$ h and 7 d) and SA24 ($H = 3.0$ m, $m = 3.0$ kg, $RR = 250$ rpm $0.5 \leq GSR \leq 0.7$ mm (90%) & $8.0 \leq GSR \leq 9.5$ mm (10%) and $t_c = 2$ h and 7 d). The influence of curing time on the strength of glass was different, leading to strength reduction in SA21 and strength increase in SA24.

Two distinct phenomena can occur in parallel but on different extents during curing: (a) changes in the chemical composition at the crack tip due to leaching of alkali [43], leading in strength increase; and; (b) sub-critical crack growth, triggered by residual surface stresses induced during impact [44], leading to strength reduction.

1% of gravel: The results show that the influence of the curing time is negligible on the mean strength (4% reduction for $t_c = 7$d, Fig. 16a). However, the influence at lower probabilities of failure is significant (38% reduction for the design strength for $t_c = 7$d, Fig. 16). The increase in curing time therefore, produces a wider distribution of strength data, manifested as a change in the gradient of the Weibull distribution (Fig. 16a) and correspondingly smaller values of the shape factor, β (Table 3). The underlying physical reasons for this response have not been investigated further, but it could be attributed to the subcritical crack growth that occurs during the curing period of the specimens as a result of the local residual stresses that are generated during impact with sand/gravel grains. This could cause flaws to grow and therefore, specimens to fail at lower stresses.

10% of gravel: The results show that with a higher percentage of gravel, increasing the curing time does lead to an increase in strength (Fig. 16b, 31% and 14% for design ($P_f = 0.008$) and mean ($P_f = 0.50$) strength respectively). It therefore, appears that the strength gains associated with curing are a function of the flaw size. In particular, larger flaws ($\alpha > 400$ μm) produce a net strengthening after curing whereas smaller flaws produce a net weakening after curing.

3.3.6.2. Influence of environmental conditions during storage. The influence of the environmental conditions (ambient or under water) during storage was found to be negligible and to produce almost identical strength results (Fig. 16b) and is in agreement with [45].

3.4. Correlation of naturally aged to sand abraded glass

Fig. 17a-d shows a detailed comparison across all the series (AR, NA and SA) that were tested in this study. Good agreement was found for the mean strength between most of the SA series and the NA glass (Fig. 17a), but there was generally poor agreement at the lower probabilities of failure commonly used in engineering design. In fact, most of the SA series overestimated the design strength by a very significant margin (Fig. 17b). Statistically, this is evidenced by the lower shape factor in naturally aged glass than most of the SA series (Fig. 17c); the shape factor represents the gradient of the distribution and therefore has a larger influence on the lower (and higher) fractile values away from the mean. Low shape factors, closer to the values found in naturally aged glass, were found for SA series with small percentages of gravel (0.1% – SA18 & 10% – SA23) and longer curing times (7 days - SA21). Additionally, NA glass had significantly larger coefficients of variation ($30 \leq CV \leq 33\%$) than most of the SA series ($4 \leq CV \leq 19\%$) that

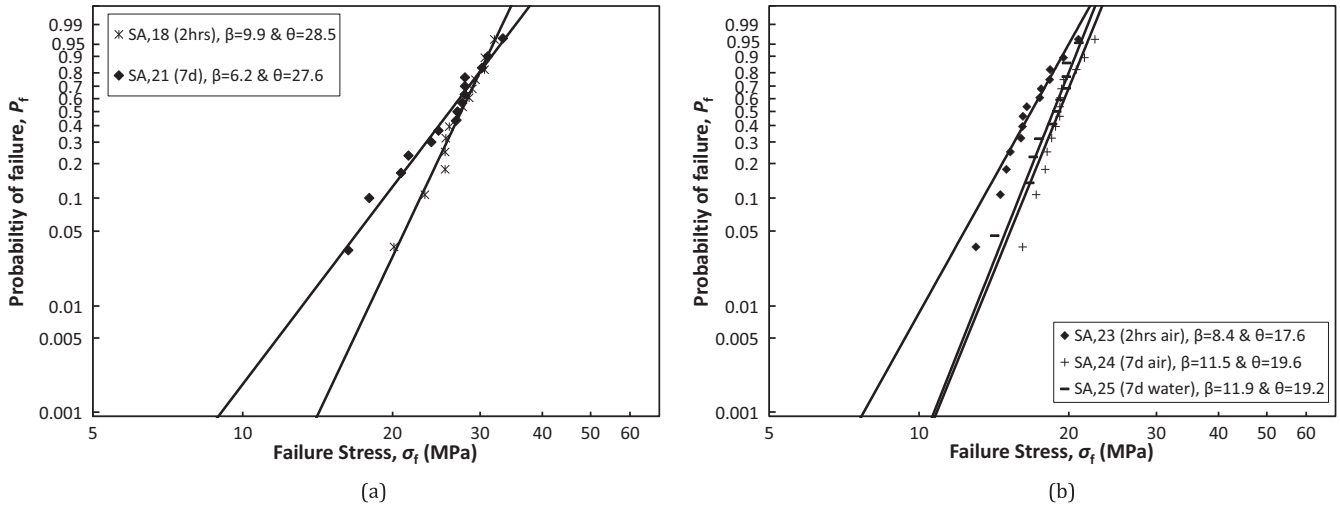

Fig. 16. Effect of curing time on the Weibull distribution for $H = 3.0$ m, $m = 3.0$ kg, $RR = 250$ rpm and; (a) $0.5 \leq GSR \leq 0.7$ mm (99.9%) & $8.0 \leq GSR \leq 9.5$ mm (0.1%) and; (b) $0.5 \leq GSR \leq 0.7$ mm (90%) & $8.0 \leq GSR \leq 9.5$ mm (10%).

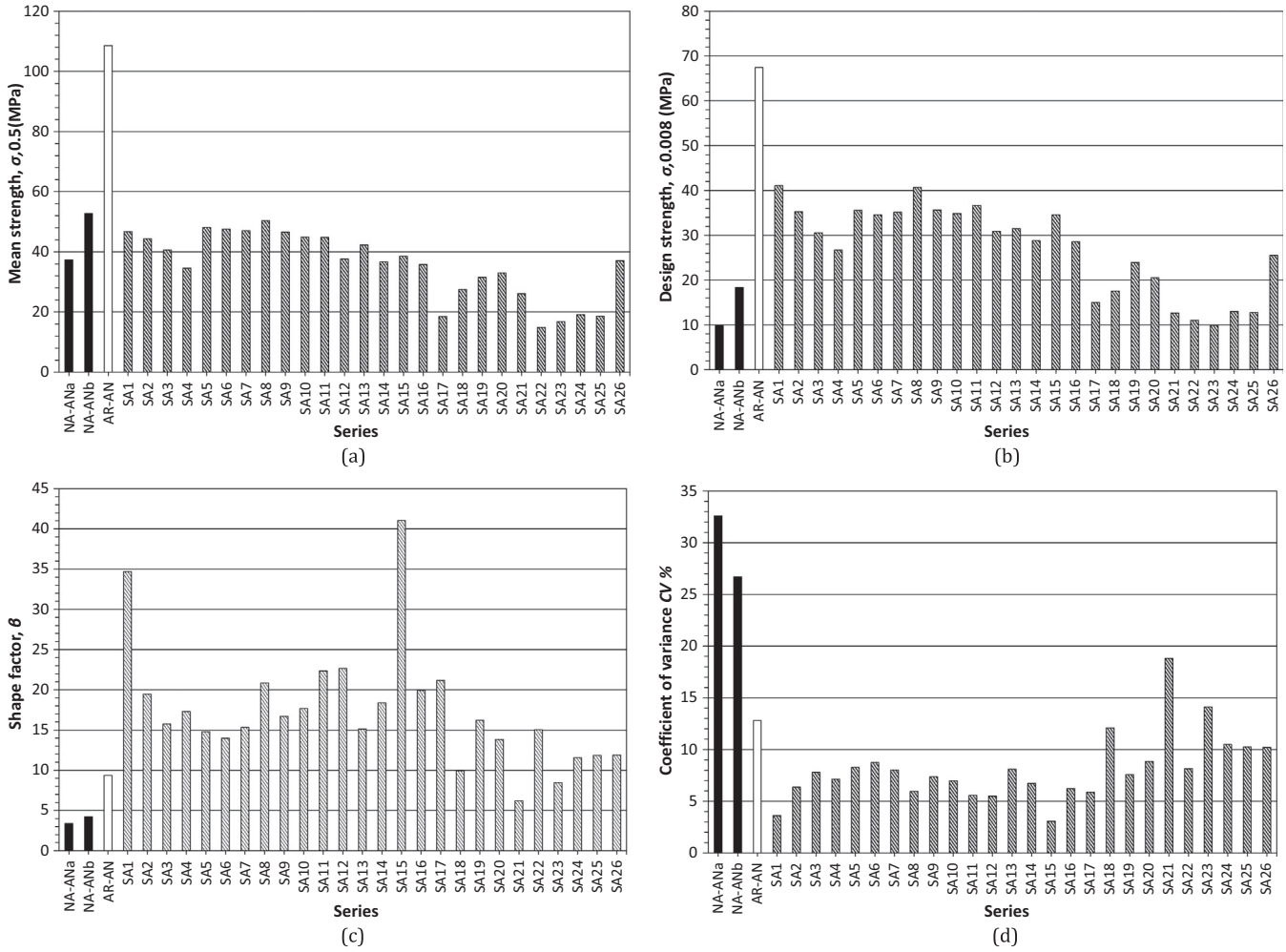

Fig. 17. Comparison of AR, NA and SA series in terms of: (a) mean strength; (b) design strength; (c) shape factor and; (d) coefficient of variance.

generally provided fairly consistent results with low scatter (Fig. 17d).

The ageing parameters prescribed in DIN 52348 [28], adopted in SA2, provide a good estimate of the mean strength of naturally aged glass but a significant overestimation of design strength ($92\% \leq \Delta\sigma_{NA,SA2}/\sigma_{NA} \leq 253\%$ for the 0.008 probability of failure). Therefore, this method is not suitable when strengths at low probabilities of failure are essential.

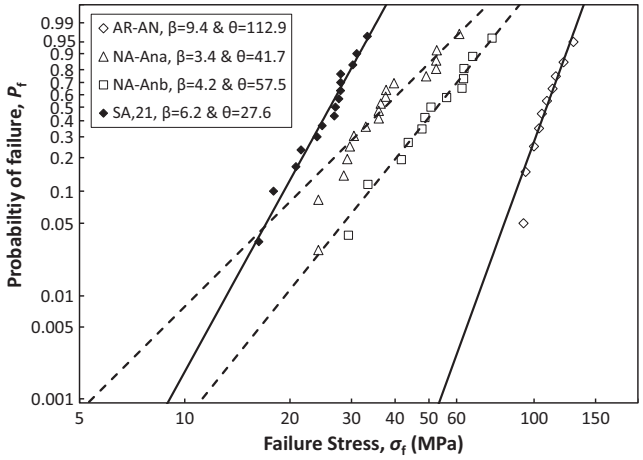

Fig. 18. CDF for NA-AN, AR-AN and best performing of SA series (SA21).

A close correlation at all probabilities of failure between the strength of naturally aged and sand abraded glass is very difficult to obtain. However, strengths at low probabilities govern engineering design and therefore, SA21 can be considered the best performing among the SA series (Fig. 17, Fig. 18 and Table 3).

4. Conclusions

This study showed that annealed glass suffered a significant reduction in its extrinsic as-received strength during its 20-year service life; a 85% reduction was found for the lower probabilities of failure, commonly used for determining design strength, in naturally aged glass. Therefore, the evaluation of the long term performance of glass (annealed, heat treated and chemically toughened) is essential. DIN 52348 [28] proposes a falling abrasive method to replicate ageing phenomena on glass. However, the level of damage induced by this method seems to be arbitrary and is not correlated with the strength of naturally aged glass. This study showed that the artificial ageing recommendations in DIN 52348 lead to a good estimation of the mean strength ($P_f = 0.5$) but a significant overestimation of strength at the lower probabilities of failure ($92\% \leq \Delta\sigma_{NA,SA2}/\sigma_{NA} \leq 253\%$) with respect to naturally aged glass of this study and is therefore unsafe.

Further investigations in this study showed that the falling abrasive method can induce similar levels of damage to that found in naturally aged glass but this requires careful selection of artificial ageing parameters (drop height, mass and grain size of

abrasive medium, rotation rate and curing time). Investigation of each artificial ageing parameter in turn, showed that drop height and maximum grain size of the abrasive medium are inversely proportional to the strength of the sand-abraded glass. The opposite applies to the rotation rate of the specimen base. Masses of abrasive medium smaller than 3 kg lead to bi-modal Weibull distributions triggered by pre-existing flaws and should therefore, be avoided while masses larger than 3 kg lead to an increase in strength attributed to surface material removal. Therefore, a mass of 3 kg is generally recommended. Additionally, the integration of a small percentage of gravel ($0.1 \leq p \leq 10\%$ of $8.0 \leq GSR \leq 9.5$ mm) and longer curing times results in larger scatter of strength data; this leads to lower estimates for $\sigma_{f,0.008}$ and lower shape factors, β, thereby providing a better correlation with the naturally aged glass. The following artificial ageing parameters: $H = 3.0$, $m = 3.0$ kg, $0.5 \leq GSR \leq 9.5$ mm (99.9% of $0.5 \leq GSR \leq 0.7$ mm & $p = 0.1\%$ of $8.0 \leq GSR \leq 9.5$ mm), $RR = 250$ rpm and $t_c = 7$ days were found to more closely reproduce the strength of naturally aged glass investigated in this study, for low probabilities of failure.

A more efficient use of glass and more effective glass treatments could eventually be achieved by selecting the glass and glass treatment that are tailored for the specific application and the corresponding surface damage expected during its service life. This could be achieved by performing further investigations, similar to those described in this study, on multiple sources of naturally aged glass, including glass that is exposed to a broad range of erosive and/or scratching action.

Acknowledgements

The authors gratefully acknowledge financial and technical support from Eckersley O'Callaghan, and financial support from the Engineering and Physical Sciences Research Council UK (EPSRC) and Onassis Foundation.

Appendix A: Grain size distribution curves

Grain size distribution curves are shown here.

Appendix B: Confidence intervals

Confidence intervals (90%) for the probability of failure were computed for all naturally aged, artificially aged and as-received series of this study based on EN 12603 [40]. The confidence intervals are sometimes erroneously used to set the limits of the true population. However, a confidence level of 90% means, that if the population is sampled multiple times and interval estimations are made in each case, 90% of the resulting intervals would bracket the true value [46]. Confidence intervals can be used to describe the level of uncertainty in the obtained data as a function of the width between the upper and the lower bound of each cumulative distribution function. This is true only when a good fit to a distribution is achieved and fixed errors are small.

The results for all series of this study are shown in Table B1 and Fig. B1a-b for design ($P_f = 0.008$) and mean strength ($P_f = 0.50$). The width of the confidence intervals can be used to assess the uncertainty in the data for the sand abraded series because fixed errors are small and constant; (a) glass was provided by the same supplier; (b) artificial ageing and destructive tests were performed by the same researcher and; (c) the testing procedure was identical for all specimens in all series. The width of the intervals for SA series is small (5.9 ± 2.8 MPa) for $P_f = 0.008$ and negligible for $P_f = 0.50$ (2.5 ± 1.9 MPa). This indicates that 15 specimens per series is sufficient to derive reliable strength results.

However, it is not possible to establish if the number of specimens is sufficient for naturally aged glass based on the width of their confidence intervals. This is because of the larger errors/uncertainties that are associated with naturally aged glass during its service life.

Appendix C: Mixed Weibull distributions

Bi-modal distributions in glass strength data occur due to different underlying causes of failure/flaw morphologies within the same data set. These series are more faithfully described by mixed Weibull distributions (Eq. C1).

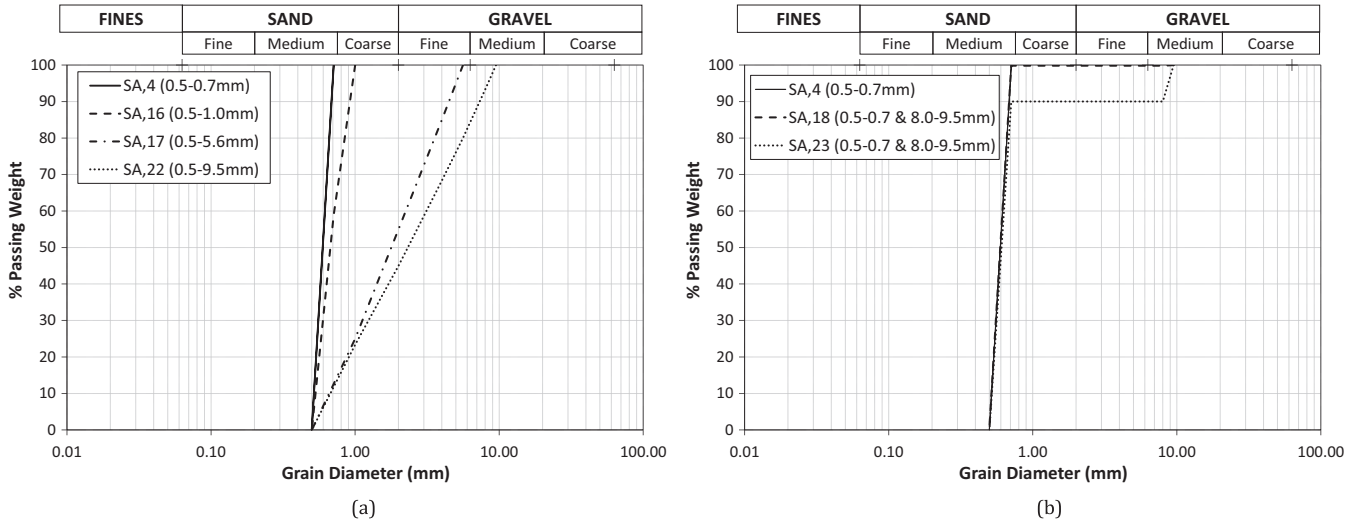

Fig. A1. Grain size distribution curves for: (a) well graded abrasive media and; (b) well sorted abrasive media.

Table B1
Confidence interval upper and lower bounds for design ($P_f = 0.008$) and mean ($P_f = 0.50$) probabilities of failure.

Series	Fractile values							
	$\sigma_{f,0.008}$ MPa	$\sigma_{f,0.008,\ up.}$ MPa	$\sigma_{f,0.008,\ low.}$ MPa	$\sigma_{f,0.008,\ up.}$-$\sigma_{f,0.008,\ low.}$ MPa	$\sigma_{f,0.5}$ MPa	$\sigma_{f,0.5,\ up.}$ MPa	$\sigma_{f,0.5,\ low.}$ MPa	$\sigma_{f,0.50,\ up.}$-$\sigma_{f,0.50,\ low.}$ MPa
NA-ANa	10.00	15.43	6.36	9.07	37.41	42.44	31.94	10.50
NA-ANb	18.36	27.24	11.39	15.84	52.76	59.49	45.34	14.16
AR-AN	67.44	81.52	52.09	29.43	108.58	115.48	100.26	15.22
SA1	41.10	43.12	38.69	4.43	46.74	48.14	45.52	2.62
SA2	35.28	38.17	31.64	6.53	44.36	45.48	43.00	2.48
SA3	30.59	33.55	26.84	6.71	40.59	41.82	39.13	2.69
SA4	26.69	29.04	23.68	5.35	34.54	35.49	33.40	2.09
SA5	35.56	39.44	30.84	8.61	48.08	49.68	46.14	3.54
SA6	34.59	38.59	29.76	8.83	47.57	49.26	45.55	3.70
SA7	35.16	38.85	30.64	8.22	47.03	48.54	45.20	3.34
SA8	40.70	44.32	36.40	7.92	50.41	51.74	48.72	3.02
SA9	35.63	39.36	31.28	8.08	46.53	47.97	44.78	3.19
SA10	34.89	38.57	30.38	8.19	44.89	46.38	43.03	3.34
SA11	36.68	39.51	33.16	6.35	44.78	45.85	43.43	2.43
SA12	30.89	33.05	28.12	4.93	37.61	38.43	36.62	1.81
SA13	31.48	34.83	27.38	7.45	42.26	43.64	40.60	3.04
SA14	28.79	31.16	25.72	5.44	36.69	37.64	35.55	2.09
SA15	34.59	35.84	32.87	2.97	38.56	39.00	38.02	0.98
SA16	28.59	30.88	25.70	5.17	35.76	36.64	34.69	1.96
SA17	15.02	16.09	13.62	2.47	18.54	18.96	18.04	0.92
SA18	17.55	20.47	14.24	6.23	27.48	28.86	25.85	3.00
SA19	23.96	26.33	21.03	5.30	31.53	32.49	30.37	2.12
SA20	25.52	27.74	22.68	5.06	32.97	33.82	31.85	1.97
SA21	12.68	16.05	9.23	6.82	26.05	28.10	23.72	4.37
SA22	11.04	12.23	9.60	2.63	14.85	15.34	14.26	1.07
SA23	9.91	11.89	7.77	4.12	16.81	17.81	15.65	2.16
SA24	13.01	14.85	10.85	4.00	19.13	19.96	18.15	1.80
SA25	12.78	14.85	10.52	4.33	18.62	19.50	17.54	1.96
SA26	25.51	28.83	21.48	7.35	37.07	38.59	35.34	3.26

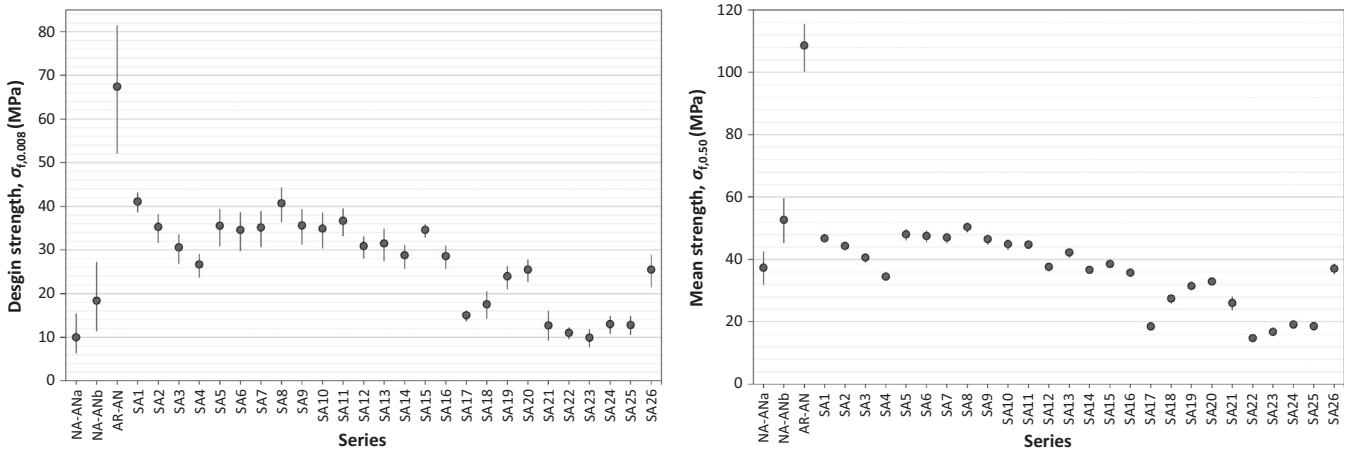

(a) (b)

Fig. B1. Upper and lower bound (based on confidence intervals) and CDF strength (dot) for: (a) design strength $P_f = 0.008$ and; (b) mean strength ($P_f = 0.50$).

$$P_f(\sigma_{f,60}) = p \cdot \left\{1 - \exp\left[-\left(\frac{\sigma_{f,60}}{\theta_1}\right)^{\beta_1}\right]\right\} + q \cdot \left\{1 - \exp\left[-\left(\frac{\sigma_{f,60}}{\theta_2}\right)^{\beta_2}\right]\right\} \quad \text{(C1)}$$

where: p and q: the mixing weights for the two Weibull distributions ($p + q = 1$).

An example of bi-modal failure is given in Fig. C1 for series SA10. The types of critical flaws were: (a) pre-existing linear scratches and; (b) digs induced during the artificial ageing process. It was found that a mixed Weibull distribution provides a better fit to the bi-modal data than a 2-parameter Weibull distribution (159% increase in goodness-of-fit).

Appendix D. Supplementary data

Supplementary data associated with this article can be found, in the online version, at http://dx.doi.org/10.1016/j.conbuildmat.2017.03.094.

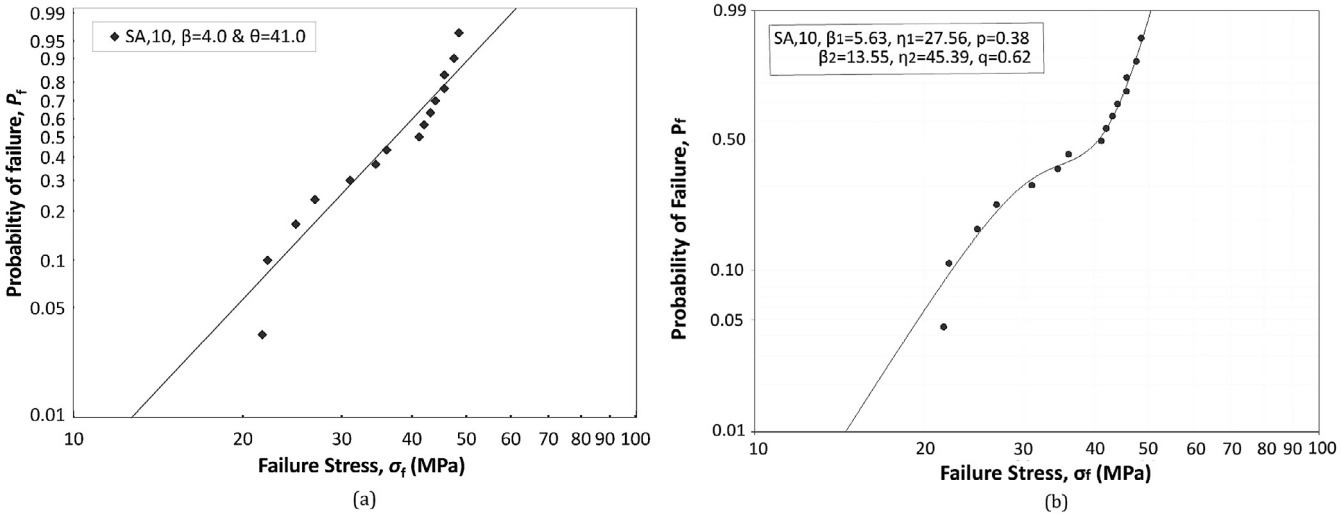

Fig. C1. CDF for bi-modal strength data described by: (a) 2 parameter Weibull and; (b) mixed Weibull distribution.

References

[1] M. Haldimann, M. Overend, A. Luible, Structural Use of Glass, International Association for Bridge and Structural Engineering, IABSE Association, ETH Zürich, 2008.

[2] K. Zammit, M. Overend, Increasing the design strength of glass - fractography and stress testing, in: International Association for Shell and Spatial Structures (IASS) Symposium, 2009.

[3] M. Overend, C. Louter, The effectiveness of resin-based repairs on the inert strength recovery of glass, Constr. Build. Mater. 85 (2015) 165–174.

[4] H.S. Norville, J.E. Minor, Strength of weathered window glass, Am. Ceram. Soc. Bull. 64 (11) (1985) 1467–1470.

[5] A. Fink, Ein Beitrag Zum Einsatz Von Floatglas Als Dauerhaft Tragender Konstruktionswerkstoff Im Bauwesen, 2000.

[6] J.J. Abiassi, The Strength of Weathered Window Glass Using Surface Characteristics, Texas Tech University, 1981.

[7] W.L. Beason, J.R. Morgan, Glass Failure Prediction Model, J. Struct. Eng. 110 (2) (1984) 197–212.

[8] B. Afolabi, H.S. Norville, S.M. Morse, Experimental study of weathered tempered glass plates from the Northeastern United States, J. Archit. Eng. 22 (3) (2016) 1–8.

[9] C. Louter, J. Belis, F. Veer, J.P. Lebet, Durability of SG-laminated reinforced glass beams: effects of temperature, thermal cycling, humidity and load-duration, Constr. Build. Mater. 27 (2012) 280–292.

[10] L. Andreozzi, S. Briccoli Bati, M. Fagone, G. Ranocchiai, F. Zulli, Weathering action on thermo-viscoelastic properties of polymer interlayers for laminated glass, Constr. Build. Mater. 98 (2015) 757–766.

[11] S.B. Bati, G. Ranocchiai, C. Reale, L. Rovero, Time-dependent behavior of laminated glass, J. Mater. Civ. Eng. 22 (4) (2010) 389–396.

[12] C. Schuler, Ö. Bucak, V. Sackmann, H. Gräf, G. Albrecht, Time and temperature dependent mechanical behaviour and durability of laminated safety glass, Struct. Eng. Int. J. Int. Assoc. Bridg. Struct. Eng. 14 (2) (2004) 80–83.

[13] C.P. Pantelides, A.D. Horst, J.E. Minor, Postbreakage behavior of heat strengthened laminated glass under wind effect, J. Struct. Eng. 119 (2) (1993) 454–467.

[14] C. Völker, D. Philipp, M. Masche, and T. Kaltenbach, "Development of a test method for the investigation of the abrasive effect of sand particles on components of solar energy systems", in 29th European PV Solar Energy Conference and Exhibition, 2014, pp. 22–26.

[15] F. Roumili, S. Benbahouche, J.-C. Sangleboeuf, Mechanical strength of soda-lime glass sandblasted by gravitation, Friction 3 (1) (2015) 65–71.

[16] S. Benbahouche, F. Roumili, R. Zegadi, Mechanical strength of tempered soda – lime – silica glass damaged by sand gravitation determined by bending with circular supports, in: XIX International Congress on Glass, 2001, pp. 286–289.

[17] N. Protopopescu, Sand Trickling Abrasion Testing of Float Glass. Some Methodological and Experimental Considerations, in: Glass Processing Days, 2001, pp. 261–265.

[18] K. C. Datsiou and M. Overend, Evaluation of Artificial Ageing Methods for Glass, in: Proc. Challenging Glass 5, 2016, pp. 581–591.

[19] N. Adjouadi, N. Laouar, C. Bousbaa, N. Bouaouadja, G. Fantozzi, Study of light scattering on a soda lime glass eroded by sandblasting, J. Eur. Ceram. Soc. 27 (2007) 3221–3229.

[20] S. Bouzid, N. Bouaouadja, Effect of impact angle on glass surfaces eroded by sand blasting, J. Eur. Ceram. Soc. 20 (4) (2000) 481–488.

[21] C. Bousbaa, A. Madjoubi, M. Hamidouche, N. Bouaouadja, Effect of annealing and chemical strengthening on soda lime glass erosion wear by sand blasting, J. Eur. Ceram. Soc. 23 (2) (2003) 331–343.

[22] A.J. Sparks, I.M. Hutchings, Transitions in the erosive wear behaviour of a glass ceramic, Wear 149 (1991) 99–110.

[23] J. Schneider, S. Schula, W.P. Weinhold, Characterisation of the scratch resistance of annealed and tempered architectural glass, Thin Solid Films 520 (12) (2012) 4190–4198.

[24] J. Schneider, H. Techen, and R. Stengler, "Determination of the scratch resistance of annealed and tempered glasses by using UST (Universal Surface Tester)", 53rd Int. Wissenschaftliches Kolloquium, no. Technische Universität Ilmenau, 2008.

[25] Y. Rodichev, Y. Yevplov, H. Soroka, F. Veer, Surface Cracked Layer and Damage Resistance of Glass under Contact Loading, in: Proc. Challenging Glass 3, 2012.

[26] V. Houerou, J. Sanglegoefu, S. Deriano, T. Rouxel, G. Duisit, Surface damage of soda – lime – silica glasses : indentation scratch behavior, J. Non. Cryst. Solids 316 (2003) 54–63.

[27] S. Schula, Charakterisierung der Kratzanfälligkeit von Gläsern im Bauwesen (PhD thesis), TU Darmstadt, 2014.

[28] DIN 52348; Deutsches Institut Fur Normung, Standard for Testing of Glass and Plastics; Abrasion Test; Sand Trickling Method., www.din.de, 1985.

[29] ASTM D968–05, Standard Test Methods for Abrasion Resistance of Organic Coatings by Falling Abrasive, ASTM Int. West Conshohocken; PA; 2010; DOI 10.1520/D0968-05R10; www.astm.org.

[30] GlasStress Ltd, Scattered Light Polariscope SCALP Instruction Manual, ver. 5.5.

[31] M.H. Krohn, J.R. Hellmann, D.L. Shelleman, C.G. Pantano, G.E. Sakoske, F. Corporation, Biaxial flexure strength and dynamic fatigue of soda – lime – silica float glass, J. Am. Ceram. Soc. 85 (7) (2002) 1777–1782.

[32] ASTM C1499–03, Standard Test Method for Monotonic Equibiaxial Flexural Strength of Advanced Ceramics at Ambient Temperature, ASTM Int. West Conshohocken; PA; 2010; 2009, DOI 10.1520/C1499-09; www.astm.org.

[33] G.D. Quinn, Fractography of Ceramics and Glasses, Office, U.S. Government Printing, Washington, 2007.

[34] Abaqus 6.12 Documentation, Analysis User's Manual. SIMULIA, 2012.

[35] R.A. Behr, M.J. Karson, J.E. Minor, Reliability analysis of window glass failure pressure data, Struct. Saf. 11 (1) (1991) 43–58.

[36] B. Bergman, Estimation of Weibull Parameters By Using a Weight Function, 1986, vol. 5, pp. 611–614.

[37] B. Faucher, W.R. Tyson, On the determination of Weibull parameters, J. Mater. Sci. Lett. 7 (1988) 1199–1203.

[38] C.-C. Liu, A Comparison Between The Weibull And Lognormal Models Used To Analyse Reliability Data (PhD thesis), University of Nottingham, 1997.

[39] K.C. Datsiou, M. Overend, Weibull statistics for glass strength, J Struct. Saf. (2016) 1–23 (under review).

[40] EN 12603, Glass in building — Procedures for goodness of fit and confidence intervals for Weibull distributed glass strength data, CEN Eur. Comm. Stand., 2002.

[41] ASTM E1300–12a, Standard Practice for Determining Load Resistance of Glass in Buildings, ASTM Int. West Conshohocken; PA; 2010; 2012, DOI 10.1520/E1300-12A; www.astm.org, pp. 1–59.

[42] Mil-Prf-13830B, Optical components for fire control instruments; General specification governing the manufacture, assembly and inspection of, U.S. Mil. Perform. Specif., 1997.

[43] E. Gehrke, C. Ullner, M. Hähnert, Fatigue limit and crack arrest in alkali-containing silicate glasses, J. Mater. Sci. 26 (20) (1991) 5445–5455.
[44] K.E. Cramer, M. Hayward, W.T. Yost, Quantification of residual stress from photonic signatures of fused silica, AIP Conf. Proc. 1581 (33) (2014) 1679–1686.
[45] F. Veer and Y. Rodichev, Corrosion effects on soda lime glass, in: Proc. Challenging Glass 2, 2010.
[46] R.B. Abernethy, The New Weibull Handbook, fifth ed., Abernethy, Robert B, Florida, 2006.